Korean J. Chem. Eng., 39(7), 1863-1871 (2022)
DOI: 10.1007/s11814-022-1122-3

pISSN: 0256-1115
eISSN: 1975-7220

Preparation of polydopamine-coated TiO_2 composites for photocatalytic removal of gaseous ammonia under 405 nm violet-blue light

Seo-Hyun Pak*, Jung Hoon Park, and Chan-gyu Park*,†**

*Envrionmental Technology Division, Korea Testing Laboratory, 87, Digital-ro 26-gil, Guro-gu, Seoul 08389, Korea
**Dongguk University, Wonheung-gwan F619, 30, Pildong-ro 1gil, Jung-gu, Seoul 08389, Korea
(*Received 7 October 2021 • Revised 30 December 2021 • Accepted 20 March 2022*)

Abstract−Although photocatalytic reactions using the ultraviolet (UV) range (particularly UV B (280-320 nm) wavelengths) is well-established, the photocatalytic effect of longer wavelengths (especially that of UVA (≥380 nm) and visible light (≥400 nm)) have only recently been studied and utilized for environmental applications. In this work, we coated polydopamine (PDA) and TiO_2 on a support and investigated the synergistic effects of the corresponding composites for the photocatalytic removal of gaseous ammonia under 405 nm violet-blue light. The PDA layer with TiO_2 was covalently attached on a ceramic ball using the drop-casting method. The roughness and functional groups of the TiO_2-PDA coated ball surfaces were verified using an infrared imaging microscope and field emission scanning electron microscope (FE-SEM). The photocatalytic activity of the obtained hybrid TiO_2-PDA coated ball for the removal of ammonia was investigated using a UV C and 405 nm LED lamp at 24 °C. The results showed that both the TiO_2 (control sample) and TiO_2-PDA coated balls successfully removed ammonia under similar experimental conditions with the 254 nm UV C lamp. Notably, the TiO_2-PDA coated ball exhibited an enhanced ammonia removal efficiency of 72% under 405 nm LED light irradiation. Thus, the TiO_2-PDA coated ball is a promising indoor air cleaning technique under LED light irradiation.

Keywords: TiO_2, Polydopamine Layer, Photocatalytic Decomposition of Ammonia, 405 nm LED Light

INTRODUCTION

Over the past two decades, heterogeneous photocatalysts with TiO_2 have attracted attention for various applications, including water splitting [1], photocatalysis [2], and the degradation of organic pollutants [3].

Particularly, the photocatalytic process of organic pollutant decomposition using TiO_2 is an attractive research topic due to the high photocatalytic performance, low cost, and non-toxicity [4,22]. TiO_2 generates electrons (in the valence band) and holes (in the conduction band) when irradiated in the UV. Excited electrons can form superoxide radical ions (O^{2-}) and holes (h^+), which can form reactive hydroxyl radicals (OH). These radicals contribute to photocatalytic reactions [5]. TiO_2 has a band gap of 3.2 eV and is mainly activated by ultraviolet radiation (UV C and UV B). To effectively utilize the visible-light constituting 40% of the solar radiation reaching the earth's atmosphere, it is essential to develop a UVA and visible-light reactive catalyst.

There has been an increase in research on application of various TiO_2 composites in the UVA (380-400 nm) and visible wavelength regions. Verbruggen et al. studied a plasmonic TiO_2 photocatalyst for the degradation of stearic acid under solar light at approximately 490 nm [6]. Vasilaki et al. investigated Ag nanoparticles/TiO_2 deposited on reduced graphene oxide (rGO) sheets and used this for the removal of methylene blue dye under visible-light irradiation [7]. Moreover, the effect of a uniform coating and strong coupling between TiO_2 and rGO for the degradation of rhodamine B have been studied by Liang and co-workers [8].

Another important factor limiting the photocatalytic utilization of TiO_2 is the low surface area and powder form of the catalyst, which makes it difficult to reuse. To solve these problems, studies have been conducted on methods to fix the photocatalyst on a stable support. Several materials, such as activated charcoal, silica, alumina, and clays, have been utilized as supports. In addition, various strategies for coating photocatalysts on appropriate supports have been implemented to improve the photocatalytic efficiency and reusability, including sputtering deposition [9], photo reduction [10], sol-gel [11], physical deposition [12], and organic polymer modification [13].

Immobilizing TiO_2 on a support by coating with a silica binder using sol-gel method is a probable way of developing a photocatalyst surface. However, these methods have not been implemented as a protocol for developing Ti substrate coatings on supports, due to the leaching of the Ti from the support in addition to problems associated with an uneven coating surface. Electrodeposition is another surface coating method that can be used to coat TiO_2 on a support to increase the photocatalytic activity; however, it is not suitable for industrial applications due to the high costs and sophisticated equipment required.

Polydopamine (PDA) is a form of dopamine, which a neurotransmitter with various catechol groups, and is used to modify organic polymers [14]. PDA has several advantages, such as a high binding

†To whom correspondence should be addressed.
E-mail: parkcg@ktl.re.kr

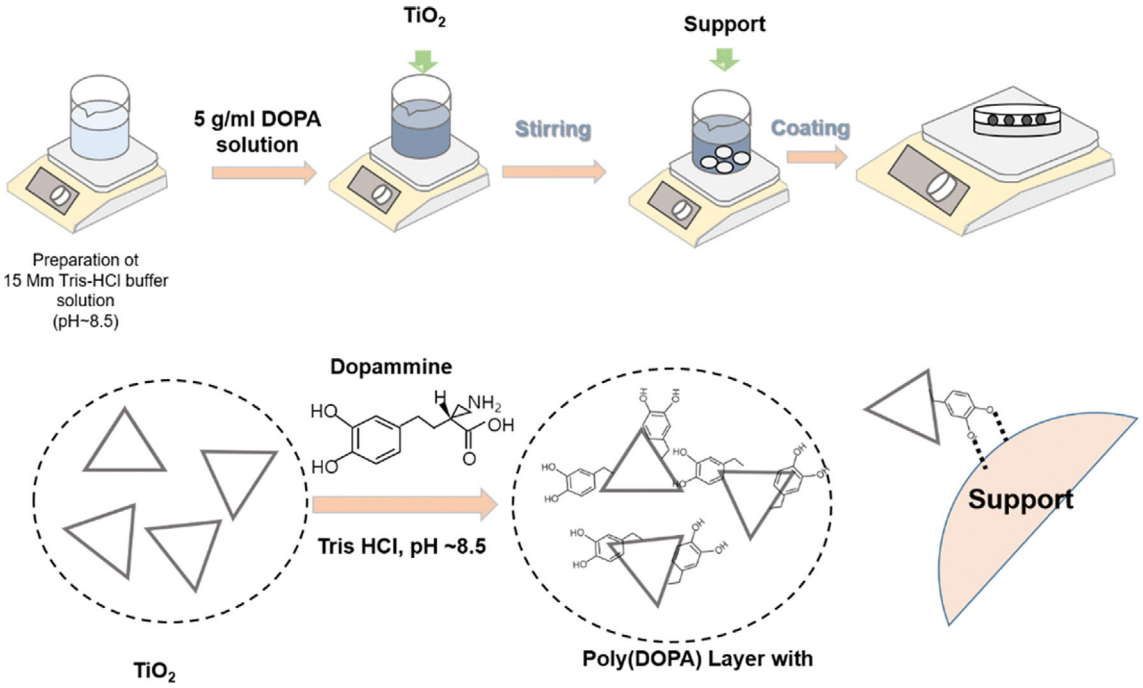

Fig. 1. Shcheme of the synthesis of PDA-Ti substrate and fabrication of PDA-TiO_2 coated on support.

strength, unique adhesive properties, low cost, and optical properties [15]. Moreover, photocatalysts with PDA have garnered significant attention due to their unique structure consisting of chelating catechol and amine groups.

Lee et al. reported surface-adherent PDA films on metals, oxides (including metal oxides), and ceramics *via* the self-polymerization of dopamine [16]. Recently, Park et al. reported that inorganic hydroxyapatite crystals form on ceramics and noble metals *via* PDA-assisted hydroxyapatite [17].

PDA is widely used for the modification of Ti implants to improve their corrosion resistance, antibacterial activity, and bioactivity [18]. The PDA layers improve the corrosion resistance and mechanical flexibility in addition to providing additional functionalities such as biocompatibility. Park et al. reported mussel-inspired functionalization of carbon nanotubes for hydroxyapatite mineralization, which greatly enhanced the formation of HA particles with biocompatibility [19].

There has been a growing interest in application of photocatalysts for odor sensing and removal. Specifically, these applications include the sensing and removal of odorous VOCs, NH_3, and GHGs [19-21]. However, there are few studies on the decomposition of ammonia using TiO_2 under UV-light (405 nm) at 24 °C. Herein, we prepared TiO_2 photocatalysts coated on ceramic balls with a PDA layer, and investigated the photocatalytic activity for the removal of VOCs (ammonia) under UV C and 405 nm LED light at 24 °C. The prepared catalysts were characterized by X-ray diffraction (XRD), scanning electron microscopy (SEM), UV-vis spectrometry, Raman spectroscopy, infrared imaging microscopy, and N_2 adsorption/desorption isotherms. The photocatalytic removal of ammonia by TiO_2/PDA/support was investigated and directly compared with the TiO_2 coated with a Si binder.

EXPERIMENTAL DETAILS

1. Materials

TiO_2 (NJ, USA) was used as the Ti substrates. Dopamine hydrochloride and tris(hydroxymethyl)aminomethane were purchased from Alfa Aeser, Tianjin, China. Before experimentation, methanol (MeOH, Sigma Aldrich, USA) and 1.0 M HCl (Samchun Pure Chemical Co. Ltd., Korea) were used to prepare the tri-base buffer solution using the following method. A buffer solution (15 mM, pH 8.5) was prepared with tris(hydroxymethyl)aminomethane, MeOH, and Deionized water (DI) and adjusted to pH 8.5 with a 1.0 M HCl solution [23].

2. Fabrication of Polydopamine-Ti Substrate Coated on Support

The treatment and subsequent steps involving PDA coating, sol deposition, and PDA-assisted TiO_2 coated on supports are illustrated in Fig. 1, Table 1, and described in the following subsections. The PDA/TiO_2/Support(X)-n, where x is the dopamine concentration (g/100 ml) and n is the number of coatings, mass, and number of moles used is summarized in Table 1. The dopamine hydrochloride solution (0.01-0.05 g/ml) was stirred with 15 mM of the tri-base buffer solution for 4 h at 60 °C in darkness. Subsequently, 0.5 g of TiO_2 was immersed in 50 mL of the dopamine solution for 4 h at 60 °C. The PDA sol with TiO_2 was coated on ceramic balls (diameter: 0.5 mm) *via* drop-casting coating. A coating solution was applied by dropping 2 mL of the solution on 10 g of ceramic balls in a glass dish at 100 °C, which was then dried in an oven at 100 °C. This process was performed thrice.

Another catalyst was coated using a silica binder to compare the performance of the PDA coating layer with other coating methods and was called the TiO_2/Support (Si binder).

Tetraethyl orthosilicate (TEOS, 98%, Sigma Aldrich, USA), dis-

Table 1. Ratio of starting materials and BET surface area for PDA-TiO_2 coated on support

	Dopa concentration (g/100 ml)	Coating material	Number of coating	Surface area (m^2/g)
Support	1	-	-	167
TiO_2/Support (si binder)	The use of Silica binder	0.5 g TiO_2 (P25)	4	112
TiO_2/PDA/Support (1)-n[a]	1	0.5 g TiO_2	1 2 4	 178
TiO_2/PDA/Support (3)-n	3	0.5 g TiO_2	1 2 4	 218
TiO_2/PDA/Support (5)-n	5	0.5 g TiO_2	1 2 4	 303

[a]TiO_2/PDA/Support (x), where x is the dopamine concentration (g/100 ml) and n is the number of coatings

tilled water, and ethanol (98%, Sigma Aldrich, USA) were used as the Si binder precursor and solvents. Nitric acid was used as a catalyst for hydrolysis. The mass ratio of the prepared Si binders was $TEOS : C_2H_5OH : HNO_3 : H_2O = 0.5 : 4 : 0.05 : 2$. After mixing the prepared binder with TiO_2 and stirring for 24 h, the final catalyst was dried in an oven at 100 °C for 24 h.

3. Characterization

The TiO_2/PDA coating on the ceramic balls was characterized by field emission SEM (FE-SEM, S-4800, Hitachi, Japan). The crystal structure and phase composition were analyzed using XRD (Ultima IV, Rigaku, U.S.A) at room temperature with Cu Kα radiation (λ=1.542 Å) within a 2θ range of 20-60°. A diffuse-reflectance UV-vis spectrophotometer (UV-DRS, JASCO V760, JASCO; Tokyo, Japan) was used to determine the band gap energy (E_g) and to identify the absorbance of the samples.

The structure, shape, and size distribution of the catalysts were observed with field emission scanning electron microscope (Fe-TEM, JEM-F200 (TFEG) (JEOL Ltd., Japan)). The surface area of the samples was characterized using the nitrogen adsorption-desorption method with a Micromeritics ASAP 2020 (Micromeritics Instrument Corporation, Norcross, Ga, USA). The surface functional groups and roughness of the samples were analyzed using a Nicolet iN10 infrared imaging microscope (Thermo Fisher Scientific, Waltham, MA, USA) from 4,000 to 400 cm^{-1}. The real time concentration of ammonia was measured with an I-Series gas analysis system (I-Series, MIDAC corporation, Costa Mesa CA, USA). Raman spectra of all samples were analyzed using a LabRam HR Evolution equipped with an optical microscope with a 10× and 100× lens and laser (532 and 785 nm).

4. Testing of Photocatalytic Activity

The obtained PDA/TiO_2/Support (5)-4 weighed 10 g. The photocatalytic activity test for the removal of gaseous ammonia by the prepared photocatalyst was performed at 24 °C using a 40 mL reactor. The gaseous ammonia was supplied at a flow rate of 0.5 ml/min using an air sampler (KAS110, KEMIK, Korea). The reactor and pump were directly connected to an I-Series gas analysis system. After the change in the ammonia concentration was established according to the amount of ammonia injected (0.1 µl) inside the manufactured test cell, the experiment was conducted by adjusting the initial concentration (7 ppm).

Seven ppm of ammonia was passed through the reactor and the ammonia inside the reactor was measured at regular intervals (20 s) using the gas analysis system (I-Series, MIDAC corporation, Costa Mesa CA, USA).

Ammonia was used as a volatile organic pollutant. The removal ratio of ammonia was determined using the following equation:

$$(\text{Ammonia})\ \text{Removal}\ (\%) = \frac{C_t}{C_0} \times 100 \quad (1)$$

Four UV C (254 nm, 8 W UV, Osram, Germany) and LED lamps (405 nm, 7.2 W UV, Greenmax, Korea) were positioned at the corners of the reactor. The total region of the LED lamp (405 nm) includes the edge of UV/visible range (380-415 nm). The distance between the lamps and reactor was 3 cm. Equal amounts of non-coated ceramic balls were used to investigate the reduction in the

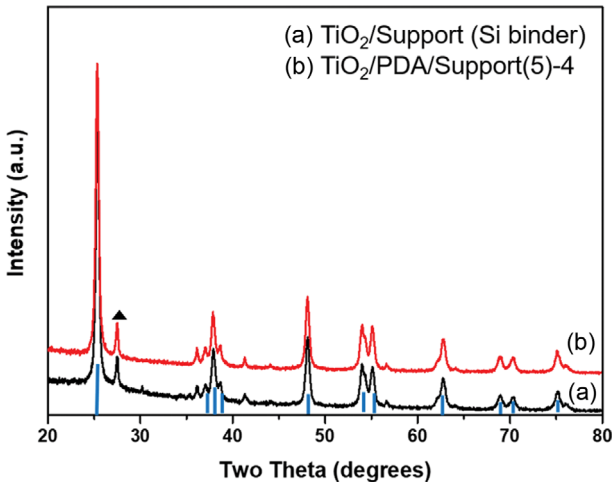

Fig. 2. The XRD patterns for TiO_2/Support (silica binder) (a) and TiO_2/PDA/Support (5) (b).

ammonia concentration for accurate comparisons. After the photocatalytic ammonia removal test, the catalyst was dried in an oven at 100 °C for 24 h. The catalysts were reused in the photocatalytic tests.

RESULTS AND DISCUSSION

1. Surface Characterization

The XRD results of TiO_2/Support (Si binder) and TiO_2/PDA/Support (5)-4 are shown in Fig. 2. The diffraction peaks of the commercial TiO_2 corresponds to that of anatase (JCPDS card no. 21-1272). The XRD pattern of all samples shows peaks at 2θ=25.1° (102), 37.6° (004), 48.0° (200), 53.9° (105), 55.1° (211), and 62.7° (310). Notably, the TiO_2/PDA/Support (5)-4 sample shows no structural changes, despite dopamine polymerization. These results indicate that the PDA and the TiO_2 were well coated on the support without any structural changes.

The UV-vis absorption spectra of TiO_2 and TiO_2/PDA/Support (5)-4 were measured from 300 to 800 nm, as depicted in Fig. 3(a). Both materials exhibit strong absorption in the UV region (200-300 nm). However, the TiO_2/PDA/support (5)-4 also exhibits absorption in the visible region (especially 380-650 nm), which was not observed for TiO_2. The absorption results for TiO_2/PDA/Support (5)-4 indicate that the TiO_2/PDA material absorbed more light in a broader range than that of pure TiO_2. The relationship between $(\alpha h\nu)^{1/2}$ and the photon energy hv was plotted, as shown in Fig. 3(b). From the Tauc plot (Fig. 3(b)), the band gap value of TiO_2/PDA/Support (5)-4 was 2.6 eV, which was smaller than the band gap energy (3.2 eV) of pure TiO_2. The reduced band gap of TiO_2/PDA/support (5)-4 compared with pure TiO_2 resulted in a red shift and thus extended the application range of UV-vis light.

Fig. 4 shows the TEM images of TiO_2, TiO_2/Support (Si binder),

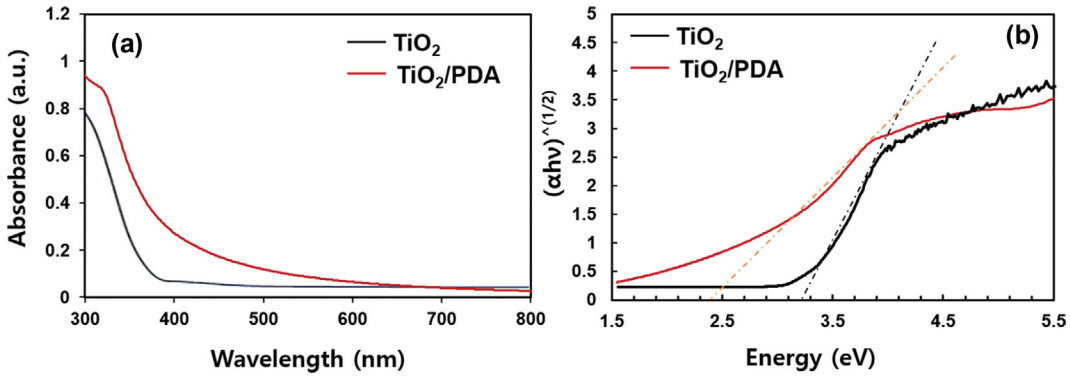

Fig. 3. The UV-vis curves (a) and plots of $(\alpha h\nu)^{1/2}$ vs Energy (eV) (b) for TiO_2 and TiO_2/PDA/Support (5)-4.

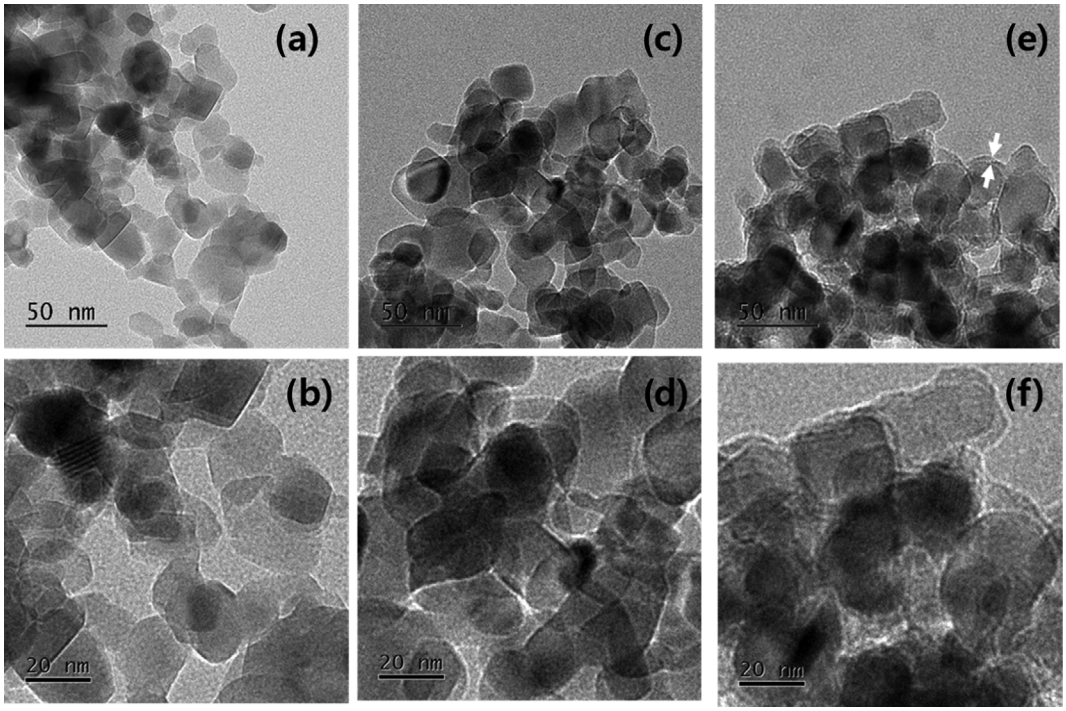

Fig. 4. The TEM images for TiO_2 (a), (b), TiO_2/Support (Si binder) (c), (d) and TiO_2/PDA/Support (5)-4 (e), (f).

and after PDA coating. TiO_2 had a slightly aggregated form and exhibited clear boundaries with angled edges (Fig. 4(a) and (b)). After coating TiO_2 with the silica binder, the TiO_2 had a similar form and clear boundaries with soft edges (Fig. 4(c) and (d)). After PDA surface coating, the agglomeration of TiO_2/PDA was enhanced slightly, due to the strong adhesion of the PDA. This is attributed

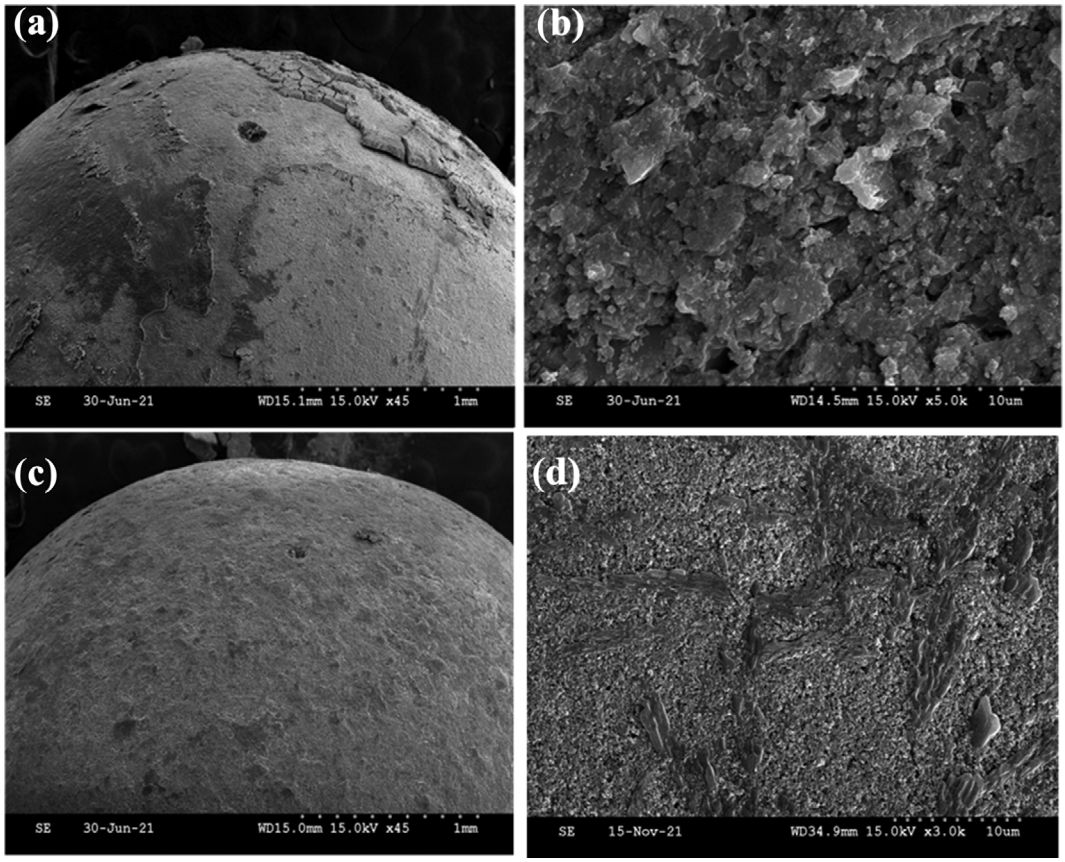

Fig. 5. SEM images of TiO_2/Support (Si binder) (a), (b) and TiO_2/PDA/Support (5)-4 (c), (d).

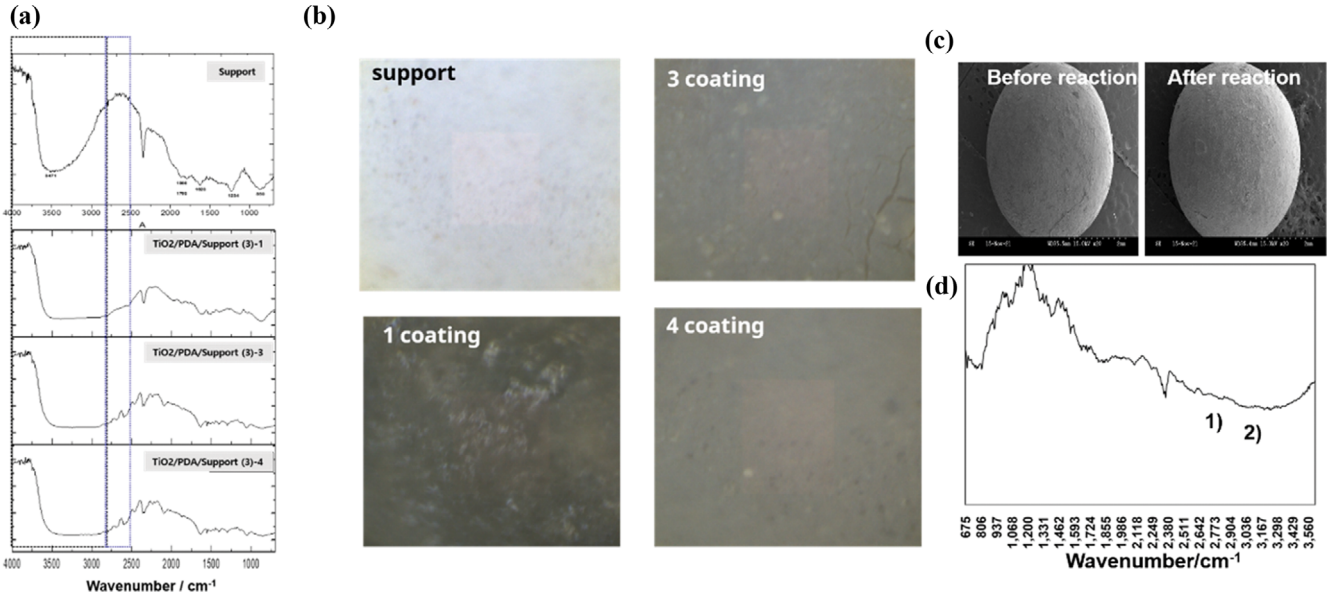

Fig. 6. IR microscopy (a) and surface imaging results (b) of TiO_2/PDA/Support (5)-n. Comparison of SEM images for TiO_2/PDA/Support (5)-4 before/after photocatalytic decomposition of the ammonia (c), FT-IR spectrum for TiO_2/PDA/Support (5)-4 after photocatalytic decomposition of the ammonia.

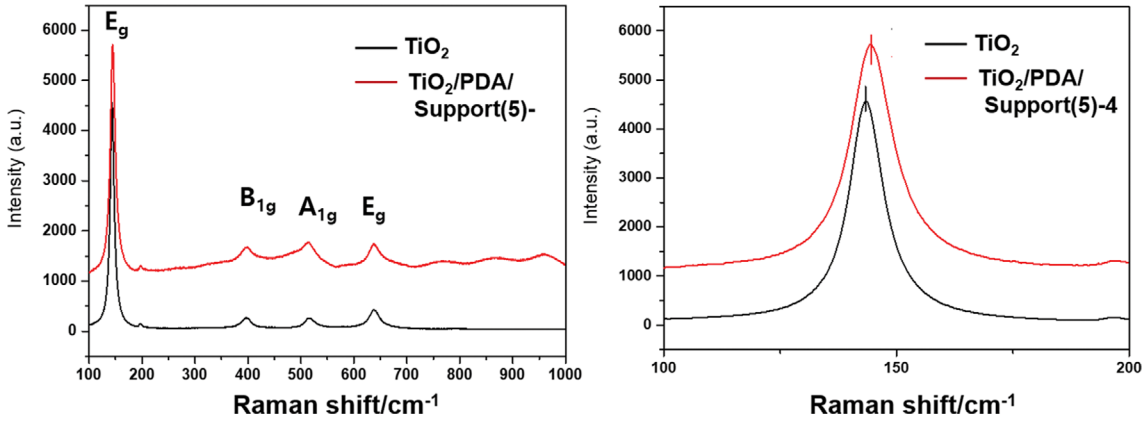

Fig. 7. Raman spectra of untreated TiO_2 and TiO_2/PDA/Support (5)-4.

to the crosslink network and catechol structure of PDA, which allows it to firmly attach to the support surfaces. The PDA coating resulted in the disappearance of the edges and corners of TiO_2, and the thickness of the coating layer was approximately 2 nm (Fig. 4(e) and (f)).

Fig. 5 presents the SEM images of TiO_2/Support (Si binder) and TiO_2/PDA/Support (5)-4. Figs. 5(a) and (b) show the surface of TiO_2/Support (Si binder), which was TiO_2 coated on the support using a Si binder. The obtained images confirm that the TiO_2 coating layer was irregular.

Figs. 5(c) and (d) show the surface of TiO_2/PDA/Support (5)-4. The PDA-TiO_2 coating on the support is clearly an excellent adhesive for both the PDA sol and Ti substrate, whereas TiO_2/Support (Si binder) shows poor interaction and cracking between the TiO_2 and support. Similar to the TEM images, after PDA surface coating, the particle agglomeration phenomenon became more evident. The analyses of PDA-TiO_2 indicate that the support was uniformly coated. The catechol group of the PDA layer acts as a nucleation site for the TiO_2 through van der Waals interactions. This strengthens the TiO_2 deposition and thus the support can be uniformly layered.

Infrared microscope imaging was performed on TiO_2/PDA/Support (5)-n to investigate the roughness of the surface and the change in the functional groups relative to the number of coatings. IR microscopy and surface imaging was simultaneously obtained using a NicoletiN10 infrared imaging microscope.

A broad peak in the 3,150-3,600 cm^{-1} range emerged owing to the hydroxyl and catechol moieties from PDA, as shown in Fig. 6(a). These results indicate that the PDA-TiO_2 layer successfully covered the support. The peaks at 2,925 and 2,852 cm^{-1} were assigned to the ν(C-H) of the PDA chain. Fig. 6(b) shows the images obtained *via* FT-IR imaging analysis of TiO_2/PDA/Support (5)-n, which demonstrates that the PDA-TiO_2 uniformly covered the support as the number of coatings increased.

Fig. 6(c) shows the SEM images before and after the ammonia photocatalytic reaction. Fig. 6(d) shows the FT-IR spectrum after the photocatalytic reaction of ammonia. From the SEM images, there is almost no change in the surface roughness of the support. From the FT-IR spectrum, the intensity of the functional group decreased, but the position of the functional group remained intact.

The Raman spectra of TiO_2 and TiO_2/PDA/Support (5)-4 are

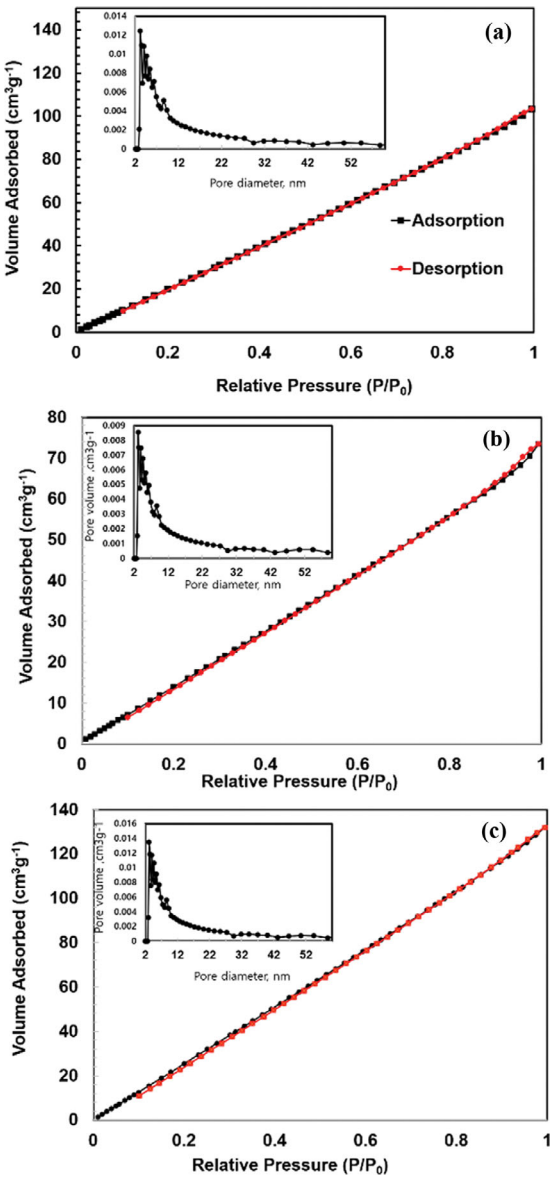

Fig. 8. N_2 sorption isotherms and pore size distribution (inlet) of support (a), TiO_2/Support (Si binder) (b) and TiO_2/PDA/Support (5)-4 (c).

shown in Fig. 7. Four peaks at 146, 405, 522, and 644 cm^{-1}, were observed for TiO_2 and TiO_2/PDA/Support (5)-4, which indicates the typical TiO_2 phase (Fig. 7(a)). The E_g peak of TiO_2/PDA/Support (5)-4 is shifted from 142 to 145 cm^{-1} due to the vibration mode changes as the coating of TiO_2-PDA layer.

Fig. 8 shows the nitrogen isotherm analysis and pore size distribution of the catalysts. A type IV isotherm with a hysteresis loop (P/P_0=0.8-0.995) was obtained, indicating the porous nature of the material. The surface area of all samples was calculated using the BET equation. The quantity of nitrogen gas absorbed was determined to be approximately 167 and 303 m^2/g for the support and the TiO_2/PDA/Support (5)-4, respectively. The increase in the surface area of the support after loading the TiO_2 and PDA layer is indicative of homogeneous coating; therefore, the surface available for nitrogen adsorption increases. The pore size distribution calculated from the isotherms in Fig. 8(a), (b), and (c) shows peaks in the range 2-12 nm for all samples.

2. Photocatalytic Removal of Gaseous Ammonia at Room Temperature

The experiment setup for the photocatalytic removal of ammonia is shown in Fig. 9. The PDA-TiO_2 coatings on the support and the TiO_2 coated directly on the support using a silica binder were examined for the photocatalytic removal of ammonia at 24 °C. In the ammonia decomposition experiments using the photocatalysts, a 254 nm lamp in the UV C region and a 405 nm lamp close to the UV A region (380-420 nm) were used.

The degradation of gaseous ammonia on a non-coated support (blank test) was determined using the same conditions for the experiment with the 254 nm lamp. The decomposition ratio of ammonia reached approximately 1% after 30 min using the non-coated support, as shown in Fig. 9(a).

Two degradation experiments were conducted of gaseous ammonia on a non-coated support (blank test) for 30 min, and the C/C_0 value of each experiment was 0.99 and 0.98. The average value was 0.9850 with a small standard deviation of 0.009. Therefore, the repeated experiments confirmed the reliability of the tests.

Fig. 9(b) shows the results of the ammonia decomposition experiment using a 254 nm UV C lamp. For the TiO_2/Support (Si binder) coated using a silica binder, the ammonia decomposition rate after 30 min was 66%, which increased to 68% for the TiO_2/PDA/Support(5)-4 coated using PDA. The improved efficiency is possibly due to the interaction between the TiO_2 and PDA coating

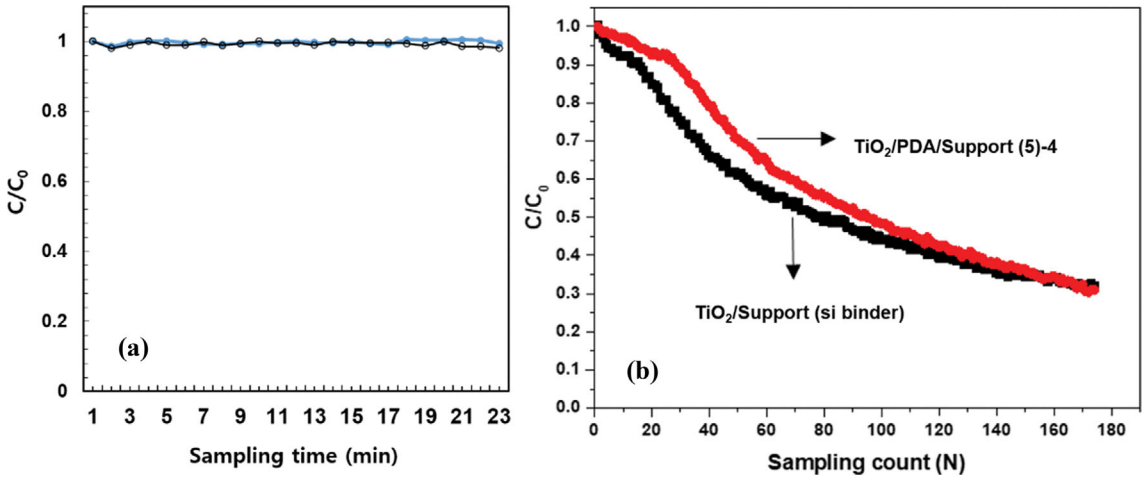

Fig. 9. Photocatalytic decomposition of the ammonia under UV light (254 nm) using non-coated support (a), TiO_2/Support (Si binder) and TiO_2/PDA/Support (5)-4 (b).

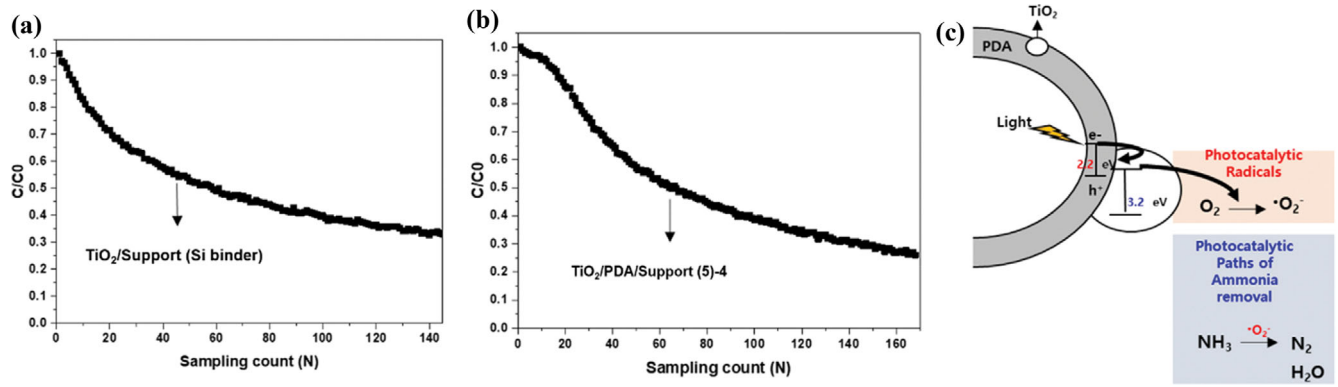

Fig. 10. Photocatalytic decomposition of the ammonia under 405 nm LED lamp using TiO_2/Support (Si binder) (a) and TiO_2/PDA/Support (5)-4 (b) and the reaction paths for Photocatalytic decomposition of the ammonia (c).

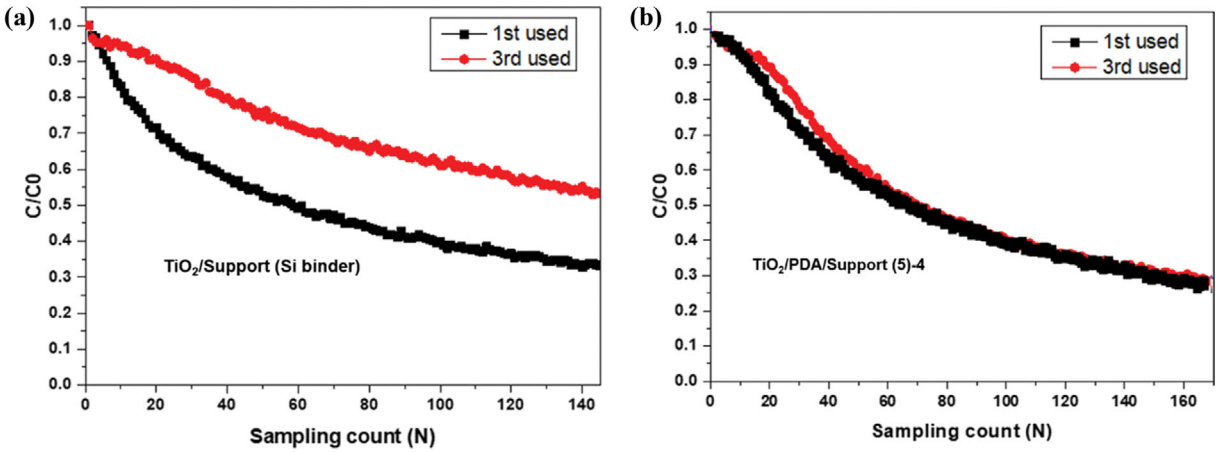

Fig. 11. Recycling test (reaction time: 30 min) for ammonia using TiO_2/Support (Si binder) (a) and TiO_2/PDA/Support (5)-4 (b).

layer, which increased the photo-catalytic activity of the existing TiO_2.

Fig. 10 shows the decomposition of ammonia by TiO_2/PDA/Support (5)-4 and TiO_2/Support (Si binder) as a function of time under irradiation with a 405 nm LED lamp. As shown in Fig. 10(a), the TiO_2/Support without the PDA layer shows a reduction rate of 65%, similar to that observed under the UV-C lamp.

A large energy of approximately 3.2 eV and wavelength of approximately 400 nm is required to activate TiO_2. The 405 nm LED lamp can supply the energy needed to activate TiO_2 because it includes the UV/visible border (380-415 nm). In addition, as the porous structure created by the combination of TiO_2 and the Si layer of the silica binder increases, the number of sites, on which photoactivity. Thus, ammonia may be decomposed even under a 405 nm LED lamp.

As shown in Fig. 10(b), the TiO_2/PDA/Support (5)-4 shows the best decomposition rate of ammonia: the decomposition rate reached 72% after 0.5 h under a 405 LED lamp. The higher activity of TiO_2/PDA/Support (5)-4 might be related to the greater surface area and visible-light adsorption ability compared with TiO_2-Si binder (4). Evidently, the PDA-TiO_2 coated support provides enhanced photoactivity due to the ability of the PDA coating surface to act as a sensitizer in the visible spectral range. As illustrated by the suggested mechanism presented in Fig. 10(c), an electron-hole pair is generated in the PDA layer due to photoexcitation and is transferred to the conduction band of TiO_2, which generates a superoxide radical that degrades ammonia.

3. Photocatalytic Stability over TiO_2/PDA/Support (5)-4

Recycling tests were performed in triplicate by drying the catalyst at 100 °C after each run/cycle. The recycling tests were conducted for 30 min for TiO_2/PDA/Support (5)-4 and TiO_2/Support (Si binder) for ammonia degradation (Fig. 11).

The catalytic performance of TiO_2/PDA/Support (5)-4 for the photocatalytic decomposition of ammonia remained stable at approximately 72 to 71% after three cycles (Fig. 11(a)). For TiO_2/Support (Si binder), the photocatalytic efficiency of ammonia was reduced from 65% to below 48% after three cycles (Fig. 11(b)). Layering PDA with TiO_2 mainly affected the adsorption and activation of the oxygen. The bandgaps of pure TiO_2 and hybrid TiO_2/PDA/Support (5)-4 were found to be 3.2 and 2.6 eV, respectively. The bandgap of TiO_2/PDA/Support (5)-4 facilitates the generation of photoexcited electrons under visible-light irradiation. In addition, the bandgap of the PDA layer (1.6 eV) also allows the absorption of visible light. Photo-generated electrons are transferred into the conduction band of TiO_2, which enhances the photocatalytic activity by producing oxygen vacancies on TiO_2/PDA/Support, finally leading to a more stable TiO_2/PDA/Support surface. This was beneficial for stabilizing and maintaining the photocatalytic activity of the catalyst.

CONCLUSIONS

A TiO_2 and PDA composite layer were successfully prepared by a drop-casting method. The TiO_2-based PDA materials displayed high photocatalytic activity for ammonia degradation under visible-light irradiation compared with the direct TiO_2 coated support (using a Si binder). The decomposition efficiency of ammonia was greater than 72% after 30 min, and the TiO_2/PDA/Support (5)-4 was stable and could be reused at least thrice.

Therefore, this work demonstrates that the synthesized TiO_2-based PDA materials exhibit high photocatalytic activity in the visible-light region and can be applied to various photocatalytic reactions with different polymerization reactions.

ACKNOWLEDGEMENTS

This work is supported by the Korea Agency for Infrastructure Technology Advancement (KAIA) grand funded by the Ministry of Land, Infrastructure and Transport (Grant 20CTAP-C157292-01).

REFERENCES

1. S. G. Sanches, J. H. Flores and M. I. P. Silva, *Mater. Res. Bull.*, **109**, 82 (2019).
2. V. Likodimos, *Appl. Catal. B.*, **230**, 269 (2018).
3. L. Zhang, L. Xu, J. He and J. Zhang, *Electrochim. Acta*, **117**, 192 (2014).

4. S. Hernández, D. Hidalgo, A. Sacco, A. Chiodoni, A. Lamberti, V. Cauda, E. Tresso and G. Saracco, *Phys. Chem. Chem. Phys.*, **17**, 7775 (2015).
5. L. Xiaoya, X. Jingang, L. Lingyuan, J. Xiang and F. Heqing, *Int. J. Polym. Mater.*, **66**, 835 (2017).
6. S. W. Verbruggen, M. Keulemans, M. Filippousi, D. Flahaut, G. V. Tendeloo, S. Lacombe, J. A. Martens and S. Lenaerts, *Appl. Catal. B.,* **156-157**, 116 (2014).
7. E. Vasilaki, I. Georgaki, D. Vernardou, M. Vamvakaki and N. Katsarakis, *Appl. Surf. Sci.*, **353**, 865 (2015).
8. Y. Liang, H. Wang, H. Sanchez Casalongue, Z. Chen and H. Dai, *Nano Res.*, **3**, 701 (2010).
9. S.-M. Chiu, Z.-S. Chen, K.-Y. Yang, Y.-L. Hsu and D. Gan, *J. Mater. Process. Technol.*, **192-193**, 60 (2007).
10. Z. M. Mahdieh, S. Shekarriz and F. A. Taromi, *Fibers Polym.*, **22**, 87 (2021).
11. A.-L. Pénard, T. Gacoin and J.-P. Boilot, *Acc. Chem. Res.*, **40**(9), 895 (2007).
12. W.-D. Münz, F. J. M. Hauzer, D. Schulze and B. Buil, *Surf. Coat. Technol.*, **49**(1-3), 161 (1991).
13. B. Mahltig and A. Fischer, *J. Polym. Sci. B Polym. Phys.*, **48**, 1562 (2010).
14. W.-Z. Qiu, H.-C. Yang and Z.-K. Xu, *Adv. Colloid. Interface Sci.*, **256**, 111 (2018).
15. G. E. Gu, C. S. Park, H.-J. Cho, T. H. Ha, J. Bae, O. S. Kwon, J.-S. Lee and C.-S. Lee, *Sci. Rep.*, **8**(1), 4393 (2018).
16. H. Lee, S. M. Dellatore, W. M. Miller and P. B. Messersmith, *Science (New York, N.Y.)*, **318**(5849), 426 (2007).
17. J.-J. Lee, I.-S. Park, G.-S. Shin, S.-K. Lyu, S.-G. Ahn, T.-S. Bae and M.-H. Lee, *Int. J. Precision Eng. Manufacturing*, **15**(8), 1647 (2014).
18. M. Lee, S. H. Ku, J. Ryu and C. B. Park, *J. Mater. Chem.*, **20**(40), 8848 (2010).
19. M. Lee, J. Wi, J. A. Koziel, H. Ahn, P. Li, B. Chen, Z. Meiirkhanuly, C. Banik and W. Jenks, *Atmosphere*, **11**(3), 283 (2020).
20. D. L. Maurer and J. A. Koziel, *Chemosphere*, **221**, 778 (2019).
21. M. Guarino, A. Costa and M. Porro, *Bioresour. Technol.*, **99**(7), 2650 (2008).
22. S. V. Kite, A. N. Kadam, D. J. Sathe, S. Patil, S. S. Mali, C. K. Hong, S.-W. Lee and K. M. Garadkar, *ACS Omega*, **6**(26), 17071 (2021).
23. N. F. Della Vecchia, A. Luchini, A. Napolitano, G. D'Errico, G. Vitiello, N. Szekely, M. d'Ischia and L. Paduano, *Langmuir*, **30**(32), 9811 (2014).